ARCHIVES OF ELECTRICAL ENGINEERING VOL. 75(1), pp. 41 –56 (2026)

DOI 10.24425/aee.2026.156801

Carbon fiber reinforced polymer shielding effectiveness against the near lightning strike magnetic component

PAWEŁ SZCZUPAK

Department of Electrical and Computer Engineering Fundamentals
Rzeszow University of Technology
Al. Powstańców Warszawy 12, 35-959 Rzeszów, Poland
e-mail: ✉ *pszczup@prz.edu.pl*

(Received: 24.06.2025, revised: 23.01.2026)

Abstract: This article describes the simulation results of the capability of typical carbon fiber reinforced composite to shield the magnetic component of lightning electromagnetic pulse, with a particular focus on near lightning strikes. The simulation model includes the proper polymer selection of the lightning strike model, the dependence of electrical properties on the change of frequency, and the effective medium approximation for the electromagnetic properties of composite materials. The simulations show that the carbon fiber reinforced polymer is ineffective in the low-frequency range. What's more, for frequencies in the range of a few hundred kilohertz to single megahertz, the amplitude of the disturbance signal increases.

Key words: carbon fiber reinforced polymer; near electromagnetic field; shielding effectiveness; simulation model

1. Introduction

Near lightning strikes are a critical environmental threat to electronic devices, especially since modern technology increasingly relies on sensitive electronics in many industries, transportation, energy, and various other fields. Lightning strikes produce a transient but highly intense electromagnetic pulse (EMP). This pulse generates an electromagnetic wave that induces currents in low-impedance and overvoltages in high-impedance circuits. It can damage electronic parts, disrupt operations, and lead to permanent failure of sensitive components such as microcircuits and memory units. The cascading effects of lightning-induced failures can disrupt services, jeopardize safety, and cause significant financial losses [1–4].

Unmanned aerial vehicles (UAVs) are increasingly used in various applications, from commercial delivery, agriculture, and environmental measurements to ensuring safety, military surveillance, and disaster response. However, their reliance on sophisticated electronics and lightweight materials makes them highly vulnerable to near-lightning electromagnetic pulses (EMPs). This transient, high-intensity phenomenon, associated with a lightning strike, poses a significant threat to UAVs functionality, safety, and operational reliability.

Near-lightning EMPs are characterized by rapid field intensity changes, with electric and magnetic field components reaching several tens of kV/m and hundreds of A/m/s (according to [5], magnetic field component can reach rates of change as high as 2.2×10^9 A/m/s and electric field component as 6.8×10^{11} V/m/s at a distance of 10 meters from a lightning strike, respectively). The wide frequency spectrum of the EMP (ranging from a few kHz up to several dozen MHz [6]) makes it particularly dangerous for unmanned aerial vehicle (UAV) electronic systems.

Modeling and simulations based on test results [6] allow us to estimate the safe distance of a drone from a ground discharge and determine the level of resistance of these devices to the LEMP, i.e., the lightning electromagnetic pulse. Relatively small UAVs, whose diameter does not exceed one meter due to short cable lengths, show greater sensitivity to the magnetic component of the LEMP, so it is natural that the author focused on it. It should be noted that the complexity of modeling a material like the CFRP in terms of its electrical properties is very high. During model development, many aspects like woven/tow heuristics, temperature/humidity/damage scaling, roughness loss term, and stacks of plies, were omitted or simplified.

2. Lightning EM field magnetic component strength

To calculate the first lightning strike magnetic component strength, some research is needed to determine the parameters of the lightning current, channel length, current wave speed through the discharge channel, and wave propagation speed. Choose the model of current, according to measurements, choose the approximation model. Those parameters are shown in Table 1.

Table 1. First strike lightning electromagnetic field simulation parameters [1, 2, 12, 13]

Parameters	Symbol	Typical value	Units
Pick current	I_0	20–200	kA
Rise time	t_r	0.5–1.5	µs
Decay time	t_d	40–100	µs
Total flash duration	t_{total}	50–100	µs
Charge transfer	Q	5–25	C
Return stroke speed	v	$(1 - 1.5) \times 10^8$	m/s
Channel length	L	1 000–8 000	m

To the magnetic component of the lightning electromagnetic wave, the simple Heidler function was chosen in order to describe channel-based current [15].

$$i\,(0,t) = \frac{I_0}{\eta}\frac{\left(\frac{t}{\tau_1}\right)^n}{1+\left(\frac{t}{\tau_1}\right)^n} e^{\left(\frac{-t}{\tau_2}\right)}. \tag{1}$$

For example, the current waveform (6.4/70 µs) can be represented with the following parameters: $I_0 = 100$ kA, $\eta = 0.93$, $\tau_1 = 16.5$ µs, $\tau_2 = 98$ µs and $n = 10$, which is shown in Fig. 1.

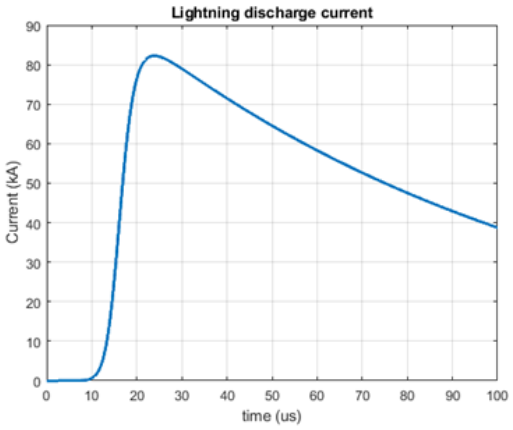

Fig. 1. Lightning discharge current waveform 6.4/70 µs

To determine the return-stroke current, one of the available models described in detail in [18] can be used. In these considerations, the modified transmission line model with exponential decay (MTLE) and modified transmission line model with linear decay (MTLL) were used. For the MTLE model, lightning channel current is given by the following equation [18–20]:

$$i\,(z',t) = e^{\frac{-z'}{\lambda}} i\left(0, t-\frac{z'}{v}\right), \quad t \geq \frac{z'}{v}, \tag{2}$$

where: z' is the height of any point in the discharge channel above the ground surface, v is the speed of the current wave (1.3×10^8 m/s), λ is the current decay height constant (determined by Nucci in 1988, equal to 2 000 m), and $i(0,t)$ is the current at the base of the lightning channel.

As for the MTLL model, lightning channel current is given by the equation:

$$i\,(z',t) = \left(1-\frac{z'}{H}\right) i\left(0, t-\frac{z'}{v}\right), \tag{3}$$

where H is the height of the return stroke channel in metres [14, 15].

2.1. Near field properties

An electromagnetic field can be divided into two types according to the distance of the observation point from the source of the wave. These are the near field and the far field. This is illustrated in Fig. 2.

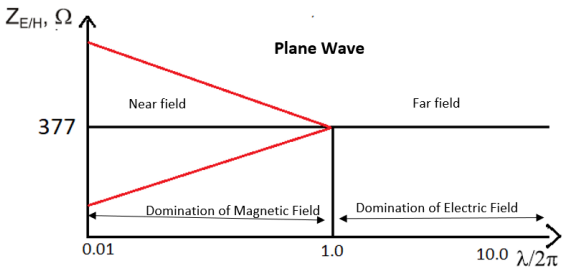

Fig. 2. Distinctive areas

In the near-field region, electromagnetic fields display intricate structures and maintain a high density of energy. Here, the characteristics of the fields are largely dictated by the specific parameters of the interference source and its surrounding environment. In this zone, electric field strength diminishes sharply, roughly following a $1/r^3$ [21] decay, while the magnetic field reduces at an approximate rate of $1/r^2$. The Fresnel region, which spans from the end of the reactive near field to about two wavelengths (2λ) away from the source, marks the transition where stored energy gradually shifts into radiated energy. Although the field structure begins to become more organized in this region, it still exhibits complex patterns, and the radiation characteristics can vary considerably with distance.

The magnetic field component with a source is the near lightning strike that can be obtained using the equation:

$$H_\phi = \frac{1}{4\pi}\int_{H-}^{H+}\left[\frac{r}{R^3}i\left(z',t-\frac{R}{c}\right)+\frac{r}{R^2c}\frac{\partial i\left(z',t-\frac{R}{c}\right)}{\partial t}\right]\mathrm{d}z', \quad R=\sqrt{(z-z')^2+r^2}, \tag{4}$$

where: R is the distance between the observation point and the height z and the channel section $\mathrm{d}z'$ at the height z', r is the horizontal distance from the observation point to the channel, L is the length of the return-stroke channel, $H+$ and $H-$ are the heights of the current front as "seen" by the observer at the time t in the channel and in its image, respectively, c is the speed of light, i is the return-stroke current.

The magnetic field can be divided into two components: H_φ(induction) and H_φ(radiation); they are given by equations:

$$H_\phi\,(\text{induction}) = \frac{1}{2\pi}\left(\frac{i\,(z',t)\,\kappa}{\sqrt{r^4\left(1+\dfrac{\kappa^2}{r^2}\right)}}\right), \tag{5}$$

$$H_\phi(\text{radiation}) = \frac{1}{2\pi}\left(\frac{i\,(z',t)}{\dfrac{c}{v}\left(\kappa^2+r^2\right)+\sqrt{\kappa^4\left(1+\left(\dfrac{r}{\kappa}\right)^2\right)}}\right). \tag{6}$$

In Eqs. (2) and (3)

$$\kappa = \frac{v\left[c^2t-\sqrt{v^2\left(ct^2-r^2\right)+(cr)^2}\right]}{c^2-v^2}, \tag{7}$$

where v is the speed of return stroke wave propagation.

The magnetic component of the lightning return stroke can be given as:

$$H_{\text{Total}} = \frac{1}{2\pi}\left[\left(\frac{i\left(z',t\right)\kappa}{\sqrt{r^4\left(1+\frac{\kappa^2}{r^2}\right)}}\right)+\left(\frac{i\left(z',t\right)}{\frac{c}{v}\left(\kappa^2+r^2\right)+\sqrt{\kappa^4\left(1+\left(\frac{r}{\kappa}\right)^2\right)}}\right)\right]. \tag{8}$$

By submitting the Taylor series expansion of $i(z',t\text{-}R/c)$ into the second term of Eq. (1) we can obtain the approximation for the induction magnetic field component as:

$$H_\phi = H_\phi\,(\text{indction}) = \frac{1}{2\pi}i\left(0,t-\frac{r}{c}\right)\int_0^H \frac{r}{R^3}dz' = \frac{1}{2\pi}i\left(0,t-\frac{r}{c}\right)\frac{H}{R(H)}. \tag{9}$$

When considering the case of magnetic fields at distances up to 1 km and electromagnetic fields at ground level, the radiation component of the magnetic field, due to its small value compared to the induced one, can be ignored. At such a short distance, it can also be assumed that $r \ll H$, so when the current propagates upward along the channel, $R(H)$ gradually approaches H. Setting $H/R(H) = 1$, Eq. (6) can be simplified to [17]:

$$H_\phi = \frac{i\left(z',t-\frac{r}{c}\right)}{2\pi r}. \tag{10}$$

For cloud-to-ground (CG) lightning, the first strike current is typically in the range from 10 kA to 200 kA, and the average peak current is about 30 kA. The simulation results of the magnetic field intensity of a cloud-to-ground discharge for selected distances from the discharge channel, assuming the worst-case scenarios (first strike current of 200 kA), are presented in Figs. 3 and 4. The highest values of the magnetic field for both models are listed in Table 2.

According to [22, 25], the MTLL model is better suited for simulating the electromagnetic field of near lightning, more accurately reproducing the actual, observed waveforms. The research results presented in the above-mentioned publication prompted the author to choose the MTLL model for further simulations. The parameters for the simulations are written in Table 3.

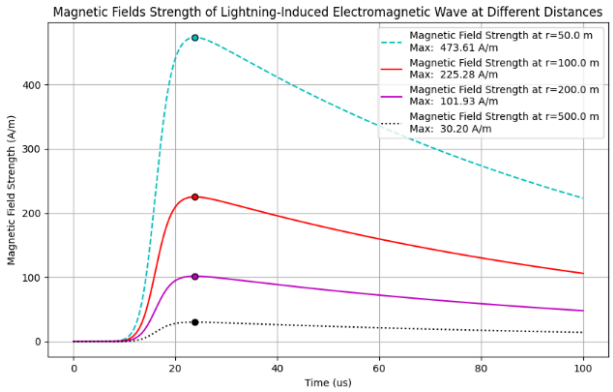

Fig. 3. Magnetic field strength for near lightning first stroke at distances of 50 m, 100 m, 200 m, and 500 m for the MTLE model

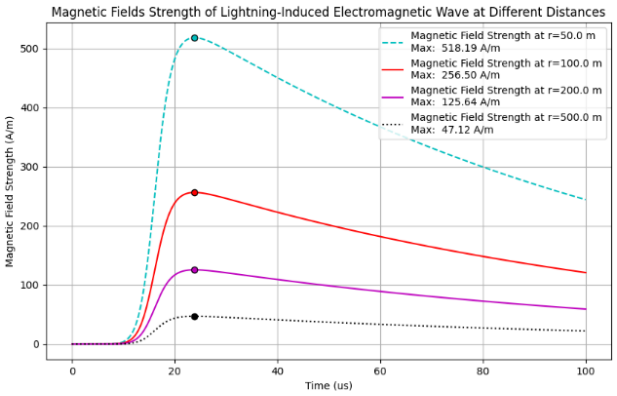

Fig. 4. Magnetic field strength for near lightning first stroke at distances of 50 m, 100 m, 200 m, and 500 m for the MTLL model

Table 2. Simulated parameters for magnetic field strength of near CG lightning strike (current 200 kA, rise time 6.4 μs, fall time 70 μs)

Distance [m]	***H* [A/m]**	
	MTLE	MTLL
50	473.61	518.19
100	225.28	256.50
200	101.93	125.44

Table 3. Chosen parameters for lightning magnetic field component simulations

Lp.	***I*$_0$ [kA]**	***r* [m]**	***t* [s]**	***H* [m]**	***v* [m/s]**
1.	10	50	1×10^{-4}	5 000	1.3×10^8
		100			
		250			
		500			
2.	30	50			
		100			
		250			
		500			
3.	100	50			
		100			
		250			
		500			
4.	200	50			
		100			
		250			
		500			

Continued on next page

Table 3 – *Continued from previous page*

Lp.	I_0 **[kA]**	r **[m]**	t **[s]**	H **[m]**	v **[m/s]**
5.	200	50		7 500	1.5×10^8
		100			
		250			
		500			

The simulation results for the parameters from Table 3 are shown in (a), (b), (c), (d) and (e) in Fig. 5.

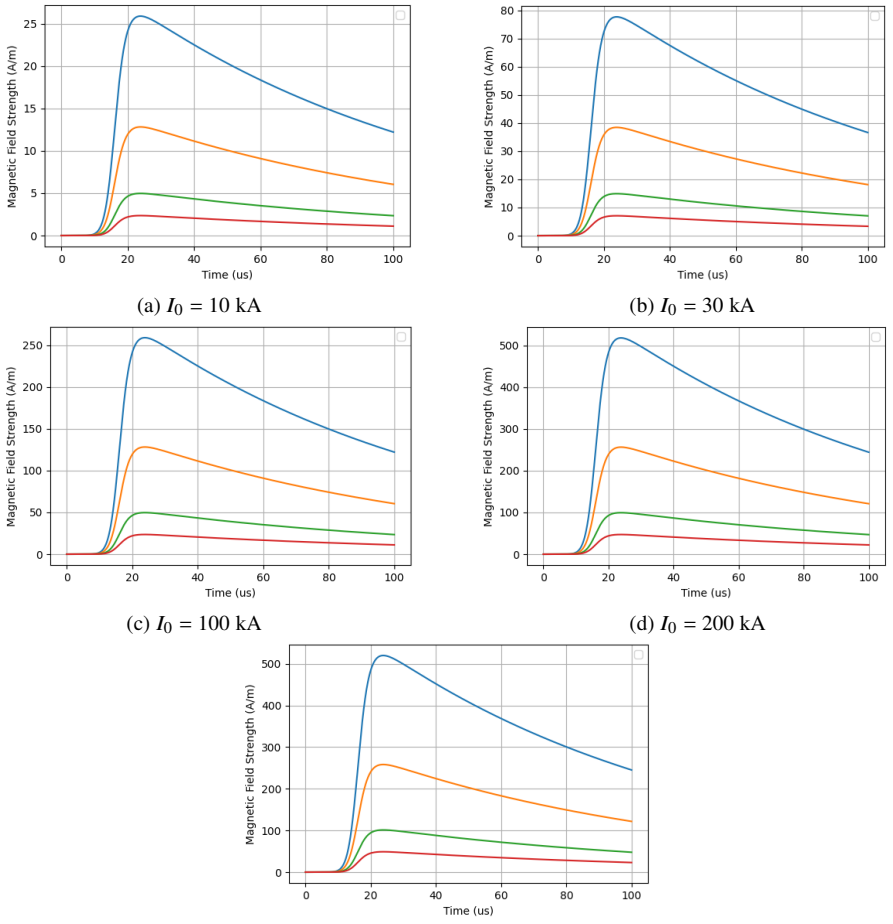

(a) I_0 = 10 kA (b) I_0 = 30 kA

(c) I_0 = 100 kA (d) I_0 = 200 kA

(e) I_0 = 200 kA

Fig. 5. Magnetic field strength simulations for: (a) I_0 = 10 kA; (b) I_0 = 30 kA; (c) I_0 = 100 kA; (d) I_0 = 200 kA and (e) I_0 = 200 kA, H = 7500 m and $v = 1.5 \times 10^8$ m/s at distances of 50 (red), 100 (green), 250 (orange), and 500 (blue) meters

Assuming the above data for the first-stroke current, the value of the magnetic field intensity for the lightning current $I_0 = 200$ kA and a distance of 500 m is approximately 47 A/m (Fig. 6).

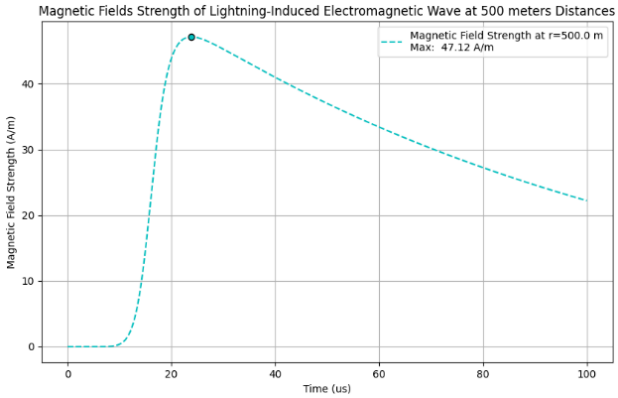

Fig. 6. Calculated magnetic field strength at a distance of 500 meters from lightning (first stroke)

Lightning currents are inherently impulsive and broadband. Their rapid rise and fall times result in a broad frequency spectrum, with significant energy concentrated in certain ranges. The key frequency components of the lightning current are:

1. Extremely low frequencies (ELF) – a few hertz, up to 100 Hz. They can propagate globally in the Earth–ionosphere waveguide, which gives rise to Schumann resonances that appear as distinct peaks near $\approx 7.8 - 7.83$ Hz (fundamental) and higher modes at roughly 14.3, 20.8, 27.3, 33.8 Hz, etc.
2. Very low frequency to low frequency (VLF/LF) – up to ~100 kHz; this band carries much energy relevant to many EMI/overvoltage and power-system coupling problems.
3. High frequency and VHF (from 100 kHz up to many MHz and above) – particularly fast, compact events such as narrow bipolar Events (NBEs) or rapid microsecond features in return strokes produce strong radiation in the MHz range and can dominate at VHF. Although the integrated energy decreases with increasing frequency, this broadband region should not be ignored because it is important for sensitive electronics and can contribute to RF interference.

3. Shielding effectiveness theory

The attenuation of electromagnetic waves by the CFRP is attributed to three mechanisms: reflection, absorption, and multiple reflections within the material. The concept of shielding effectiveness for a slab of conductive material is shown on Fig. 7.

a) **Reflection**

Reflection loss occurs at the interface between air (or another medium) and the CFRP, driven by the impedance mismatch. Since CFRP's surface conductivity is high, a greater mismatch with the surrounding medium enhances reflection.

b) **Absorption**

Inside the material, EM energy converts to heat. Absorption depends on the material's electrical conductivity (σ), magnetic permeability (μ), thickness (d), and the frequency (ω) of the incident

wave. The absorption coefficient α is given by:

$$\alpha = \sqrt{\frac{\omega\mu\sigma}{2}}, \tag{11}$$

where: α is the absorption coefficient, ω is the pulsation of the incident wave, $\omega = 2\pi f$, where f is the frequency, μ is the magnetic permeability and σ is the electrical conductivity.

c) **Multiple internal reflections**

When the CFRP contains heterogeneous structures (e.g., fillers or fiber bundles), internal reflections lead to additional attenuation through phase cancellations. The effectiveness depends on the microstructure, including fiber orientation and filler content.

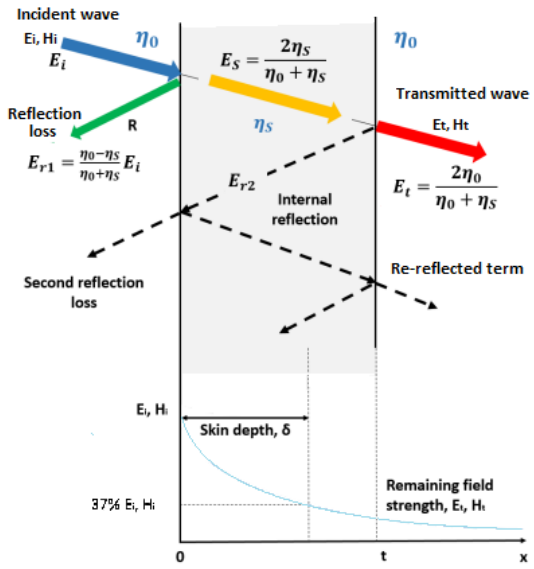

Fig. 7. Concept of shielding effectiveness (SE) for a slab of conductive material, wave absorption, reflection, re-reflection and transmission mechanisms. E_S is the transmitted wave at the first interface and E_r is the reflected wave [23]

3.1. Factors influencing shielding effectiveness

- Material Properties: conductivity, permittivity, permeability, and composite microstructure.
- Geometric Factors: sample thickness, fiber orientation, and layering (multilayer stacks).
- External Conditions: frequency range, angle of incidence, and temperature.

I. Anisotropy in EMI Shielding

The orientation of carbon fibers within CFRPs leads to anisotropic electrical conductivity, meaning the material's ability to conduct electricity varies with direction. This anisotropy significantly affects the EMI shielding effectiveness. For instance, unidirectional CFRP composites exhibit different shielding performances based on the angle of the incident electromagnetic wave relative to the fiber orientation. Studies have shown that the electrical conductivity and, consequently, the EMI shielding effectiveness can be predicted based on the fiber orientation angle. Along the fiber direction, the CFRP exhibits high conductivity, (around 60 000 S/m – the conductivity of the carbon fibers). The conductivity through the thickness is often in the range of 10^{-3} S/m, so it is significantly lower. The factors that are affecting conductivity are [35]:

Fibers orientations,
– Matrix material – the polymer's insulating nature,
– Fiber – matrix interface (the adhesion and bonding between the fibers and matrix),
– Interlayer regions

II. Skin depth consideration

The skin depth (δ) [35] is a critical parameter that defines how deeply electromagnetic waves can penetrate into a conductive material. It is given by:

$$\delta = \sqrt{\frac{2}{\omega\mu_0\mu_r \mathrm{Re}(\sigma\,(\omega))}}, \tag{12}$$

where: δ is the skin depth, $\mathrm{Re}(\sigma(\omega))$ is the real part of the frequency-dependent conductivity, ω is the angular frequency of the incident wave, μ_r is the relative permeability, and μ_0 is the permeability of free space ($4\pi \times 10^{-7}$).

3.2. Shielding effectiveness formulas

The degree of impedance mismatching between the shielding material (η_m) and the wave propagation medium (η_0) determines the magnitude of the reflection loss ($\mathrm{SE_{Ref}}$) [16, 19].

a. Reflection loss

$$\mathrm{SE_{Ref}} = 20\log_{10}\left(\frac{(\eta_m+\eta_0)^2}{4\eta_m\eta_0}\right). \tag{13}$$

Assuming that $\eta_m \ll \eta_0$, the $\mathrm{SE_{Ref}}$ can be obtained from the equation:

$$\mathrm{SE_{Ref}} = 20\log_{10}\left(\frac{\eta_0}{4\eta_m}\right). \tag{14}$$

The impedance η, can be calculated from:

$$\eta = \sqrt{\frac{j\omega\mu}{\sigma(\omega)+j\omega\varepsilon(\omega)}}, \tag{15}$$

where: ω is the pulsation in rad/sec, μ is the magnetic permeability, $\varepsilon(\omega)$ is the permittivity, and $\sigma(\omega)$ is the electrical conductivity. For free space – $\eta_0 = 377\ \Omega$ [28, 29].

As the electrical conductivity of the material decreases, the part of the wave that penetrates the material increases and the part of the reflected wave decreases.

b. The absorption loss:

$$\mathrm{SE_{Abs}} = 20\log_{10}\left(e^{-\frac{d}{\delta(\omega)}}\right). \tag{16}$$

c. The multiple – reflection loss

$$\mathrm{SE_{MuR}} = 20\log_{10}\left|1-\frac{(\eta_m-\eta_0)^2}{(\eta_m+\eta_0)^2}e^{-\frac{2d}{\delta}}\right|. \tag{17}$$

The remaining part of the electromagnetic radiation is transmitted through the shielding material.

The total shielding effectiveness (SE) can be obtained from:

$$\mathrm{SE_{all}} = \mathrm{SE_{Ref}} + \mathrm{SE_{Abs}} + \mathrm{SE_{MuR}}. \tag{18}$$

When measurements are made, shielding effectiveness is obtained by dividing the value of the transmitted signal and the forcing signal (the signal from the source of the interference):

$$\mathrm{SE_{all}} = 20\log_{10}\frac{E_{\mathrm{out}}}{E_{\mathrm{in}}} = 20\log_{10}\frac{H_{\mathrm{out}}}{H_{\mathrm{in}}}, \tag{19}$$

where: E is the electric field and H is the magnetic field strength, and "in" and "out" indicate the transmitted values, respectively.

To simulate the shielding effectiveness of the CFRP, the model in Python was built. It includes parameters for the polymer matrix, such as high-frequency dielectric constant relaxation time in seconds, parameters for the carbon fibers: real part of fiber dielectric constant and electrical conductivity of the fiber in S/m, and it takes into consideration the multilayer CFRP stack (Tab. 4).

Table 4. Parameters used in simulation model

High-frequency dielectric constant	2.95
Characteristic relaxation time in seconds	$1 \times 10^{-7} - 3 \times 10^{-7}$
Relaxation strength	2–4
Broadening exponent ($0 \leq \alpha \leq$)	0.1–0.3
The volume fraction of inclusions in the matrix ($0 \leq \mathrm{vol_{frac}} \leq 1$)	0.6

To describe how the CFRP responds electrically to an alternating electric field over a range of frequencies, the multi-relaxation (multi Cole–Cole) model was used. In the Cole-Cole model, the complex permittivity is expressed as [36]:

$$\varepsilon(\omega) = \varepsilon_{\mathrm{in}f} + \sum_{j=1}^{n}\frac{\Delta\varepsilon_j}{1 + \left(i\omega\tau_j\right)^{1-\beta_j}} - i\frac{\sigma_{(\omega)}}{\omega\varepsilon_0}, \tag{20}$$

where: $\varepsilon(\omega)$ is the complex permittivity as a function of angular frequency ω, ε_∞ is the permittivity at infinite frequency, $\Delta\varepsilon_j = \varepsilon_{sj} - \varepsilon_{\infty j}$ is the relaxation strength of the j-th process, τ_j is the relaxation time of the j-th process, β_j is the Cole–Cole distribution parameter ($0 \leq \beta_j < 1$) describing broadening of the relaxation, $\sigma_{(}\omega)$ is the conductivity (an optional term, often added to include conduction loss of polymer or composite materials with fillers, which conduct electricity), and ε_0 is the vacuum permittivity.

For constrained carriers (e.g., fragmented pathways, contact/back-scattering), the Drude conductivity improves complex frequency-domain behavior:

$$\sigma_{(\omega)} = \frac{\sigma_0}{1 - j\omega\tau}, \tag{21}$$

where σ_0 is the DC conductivity and τ is the velocity relaxation time.

To estimate the effective dielectric permittivity of the CFRP, the Maxwell–Garnett function can be used [28,30]. The formula for the effective permittivity (ε_{eff}) according to the Maxwell–Garnett theory for anisotropic inclusion is:

$$\varepsilon_{\text{eff}} = \varepsilon_{hst} \frac{\left[1 + f_{\text{vol}} \left(\frac{(\varepsilon_{\text{inc}} - \varepsilon_{hst})}{\varepsilon_{hst} + L_i (\varepsilon_{\text{inc}} - \varepsilon_{hst})} \right) \right]}{\left[1 - f_{\text{vol}} \left(\frac{(\varepsilon_{\text{inc}} - \varepsilon_{hst})}{\varepsilon_{hst} + L_i (\varepsilon_{\text{inc}} - \varepsilon_{hst})} \right) \right]}, \tag{22}$$

where: ε_{hst} is the permittivity of the host medium and is equal to $\varepsilon(\omega)$ from (8), $\varepsilon_{\text{in}\,c}$ is the permittivity of the inclusion material, f_{vol} is the volume fraction of the inclusions within the composite, and L_i is the depolarization factor ($0 < L_i < 1$). Assuming that the fibers are oriented along the z-axis and needle-like limit, $L_x = L_y = 1/2$, $L_z = 0$.

The anisotropic permittivity tensor for the CFRP is as follows:

$$\varepsilon_{\text{eff}} = \begin{bmatrix} \varepsilon_{\text{eff},x} & 0 & 0 \\ 0 & \varepsilon_{\text{eff},y} & 0 \\ 0 & 0 & \varepsilon_{\text{eff},z} \end{bmatrix}. \tag{23}$$

In practical applications, a composite material in which the matrix and/or inclusions exhibit Cole–Cole type dispersive behavior can be modeled by representing each constituent with an appropriate Cole–Cole function. Subsequently, the Maxwell–Garnett formulation is employed to determine the composite's effective permittivity. This integrated approach enables the simultaneous consideration of the microscopic relaxation phenomena and the macroscopic influences arising from material heterogeneity.

For high frequencies or near percolation, it is necessary to apply percolation correction for conductivity. To include displacement currents:

$$\sigma(\omega) = \sigma'(\omega) + j\sigma''(\omega) = \sigma_{\text{con}}(\omega) + j\omega\varepsilon_0\varepsilon_{\text{eff}}(\omega). \tag{24}$$

For the epoxy (matrix), $\sigma_{\text{con}} \approx 0$. For carbon fibers, σ_{con} is large and weakly dispersive across microwaves, it is caused by the skin effect, which changes current distribution but not bulk σ. For DC percolation baselines, near the percolation threshold ϕ_c for the conducting phase (paths in the measured direction):

a) Above thresholds:

$$\sigma_{\text{DC}} = \sigma_{\text{fiber}} (\phi - \phi_c)^{-s}, \tag{25}$$

b) Below thresholds:

$$\sigma_{\text{DC}} = \sigma_{\text{matrix}} (\phi - \phi_c)^{t}, \tag{26}$$

where t and s are critical exponents. Typical 3D values of those exponents are $t \approx 1.6 - 2.0$, $s \approx 0.7 - 1.0$. In the case of a conductor-insulator mixture, $\sigma_{\text{fiber}} = 0$.

For AC scaling near ϕ_c the conductivity is equal to:

$$\sigma(\phi, \omega) \propto (\phi - \phi_c)^t \Phi \pm j\omega \left((\phi - \phi_c)^{-(s+t)} \right), \tag{27}$$

where Φ is the universal scaling function.

To cover the entire ϕ range (not only asymptotically near ϕ_c), McLachlan's general effective medium (GEM) Eq. (28), was used.

$$(1-\phi)\frac{\left(\sqrt[t]{\sigma_{\text{matrix}}}-\sqrt[t]{\sigma_{\text{eff}}}\right)}{\sqrt[t]{\sigma_{\text{matrix}}}+C\sqrt[t]{\sigma_{\text{eff}}}}+\phi\frac{\left(\sqrt[t]{\sigma_{\text{fiber}}}-\sqrt[t]{\sigma_{\text{eff}}}\right)}{\sqrt[t]{\sigma_{\text{fiber}}}+C\sqrt[t]{\sigma_{\text{eff}}}}=0,\quad C=\frac{1-\phi_c}{\phi_c}, \tag{28}$$

where σ_{eff} is the composite's effective conductivity, while ϕ_c and t are fitting parameters related to percolation behavior.

This form allows one to solve (typically numerically) σ_{eff} given known constituent properties and volume fraction [37, 38].

The wave number k_{CFRP} in the carbon fiber reinforced polymer is related to the attenuation of an electromagnetic wave within that material, which directly affects the absorption coefficient. It is given by:

$$k_{\text{CFRP}}=\omega\sqrt{\mu_0\mu_r\varepsilon_0\varepsilon_{\text{eff}}}. \tag{29}$$

The attenuation coefficient for absorption loss is given by the equation:

$$\alpha=\omega\left[\frac{\mu_0\varepsilon_0}{2}\left(\sqrt{(\text{Re}\,[\varepsilon_{\text{eff}}])^2+(\text{Im}\,[\varepsilon_{\text{eff}}])^2}-\text{Re}\,[\varepsilon_{\text{eff}}]\right)\right]^{\frac{1}{2}}. \tag{30}$$

The final result of the simulation is a waveform showing the effectiveness of CFRP protection against electromagnetic radiation in the frequency range from 100 kHz up to 10 MHz and 1 MHz to 1 GHz for selected parameters of the composite (Figs. 8 and 9).

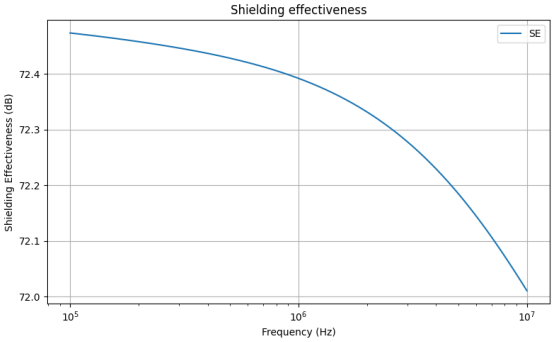

Fig. 8. Shielding effectiveness of carbon fiber reinforced polimer in frequency range 100 kHz up to 10 MHz (resolution – 100 Hz)

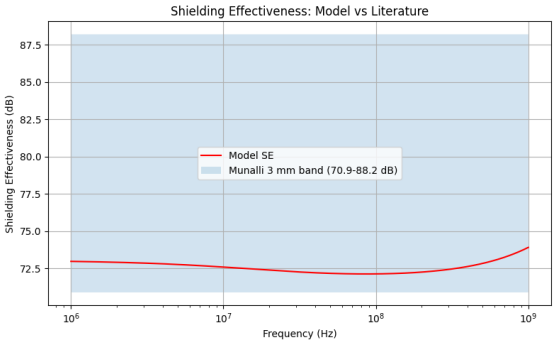

Fig. 9. Shielding effectiveness of carbon fiber reinforced polimer in frequency range 1 MHz up to 1 GHz (resolution – 100 kHz)

The simulations performed show that a typical CFRP exposed to electromagnetic radiation of a certain frequency behaves differently for different wave frequencies. For lower frequencies (from a few hundred hertz to several megahertz), the signal is amplified, which can cause damage to the electronics we want to protect [32–34]. On the other hand, above several hundred MHz, the higher the frequency, the better the interference signal is attenuated, which coincides with the findings of other researchers. The results were compared with [39, 40]. Also, simulated waveforms show a resemblance to the experimental results reported in [41], particularly with respect to the amplitude variation dynamics across the corresponding frequency intervals. Further work on the development of the simulation model will allow for an even more accurate representation of the physical phenomena occurring in the discussed material and will support the development of a material based on carbon fibers that protect electronics against LEMP pulses.

4. Conclusions

Based on the simulations presented, it can be concluded that carbon fiber reinforced polymer (CFRP) enclosures provide excellent electromagnetic shielding effectiveness at frequencies above a few megahertz, with steadily increasing SE values that make them highly suitable for protecting electronics against the high-frequency components of near-lightning EMPs. However, at very low frequencies (below ~1 MHz), the CFRP may offer limited or even negative attenuation, effectively amplifying incident magnetic fields and emphasizing the need for supplementary mitigation strategies when low-frequency EMP components are of concern. The modified transmission line with linear current attenuation (MTLL) model reproduces near-field current waveforms and resulting magnetic fields more accurately than the MTLE model, establishing it as the preferred choice for near-strike EMP simulations. In UAV applications, CFRP enclosures offer a weight-efficient solution for magnetic shielding, but anisotropic conductivity and fiber orientation must be considered to optimize protection, particularly in the critical 1–10 MHz range. Furthermore, introducing conductive or magnetic interlayers within CFRP stacks shows promise for enhancing low-frequency absorption and reducing amplification effects, pointing to a potential direction for future material innovation.

When creating the simulation model, the author was aware of the complexity of modeling a material like the CFRP in terms of its electrical properties. During the model development, many aspects were omitted or simplified. The next step will be to expand the existing model to include these aspects.

References

[1] Rakov V.A., Uman M.A., *Lightning: Physics and Effects*, Cambridge, UK, Cambridge University Press (2003).

[2] Uman M.A., *The Lightning Discharge*, New York, NY, USA, Academic Press (1987).

[3] Hong J., Xu P., *Electromagnetic interference shielding anisotropy of unidirectional CFRP composites*, Materials (Basel), vol. 14, no. 8, 1907 (2021), DOI: 10.3390/ma14081907.

[4] Chen Z.C., Wang X., An T., Zhang F., Peng Y., Li A., Liu L., *Structure-function integrated design of electromagnetic interference shielding and mechanical properties of 2D carbon fiber reinforced polymer composites based on absorption loss regulation*, Polymer Composites, vol. 46, pp. 2176–2189 (2024), DOI: 10.1002/pc.29097.

[5] MIL-STD-464C, *Electromagnetic environmental effects requirements for systems* (2010).

[6] Szczupak P., Kossowski T., *Response of drone electronic systems to a standardized lightning pulse*, Energies, vol. 14, no. 6547 (2021), DOI: 10.3390/en14206547.

[7] Cummins K.L., Murphy M.T., *An overview of recent advances in lightning location systems*, IEEE Transactopns Electromagnetic Countability, vol. 51, no. 3, pp. 499–518 (2009), DOI: 10.1109/TEMC.2009.2023450.

[8] Ibeobi S., Pan X., *Study of electromagnetic pulse (EMP) effect on surveillance unmanned aerial vehicles (UAVs)*, Journal of Mechanical Engineering, Automation and Control Systems, vol. 2, no. 1, pp. 44–53 (2021), DOI: 10.21595/jmeacs.2021.21926.

[9] Cooray V., Rubinstein M., Rachidi F., *Modified Transmission Line Model with a current attenuation function derived from the lightning radiation field – MTLD model*, Atmosphere, vol. 12, no. 2, 249 (2009), DOI: 10.3390/atmos12020249.

[10] Belousov A.O., Zhechev Y.S., Chernikova E.B., Nosov A.V., Gazizov T.R., *UAVs Protection and Countermeasures in a Complex Electromagnetic Environment*, Complexity, vol. 1, 8539326 (2022), DOI: 10.1155/2022/8539326.

[11] Kossowski T., Kwiatkowski B., Mazur D., Beňa L'., Čonka Z., Pálfi J., *Interference protection from lightning discharges associated with type of unmanned aerial vehicle shield*, Measurement, vol. 241, 115621 (2025), DOI: 10.1016/j.measurement.2024.115621.

[12] Chowdhuri P. *et al*., *Parameters of lightning strokes: a review*, IEEE Transactions on Power Delivery, vol. 20, no. 1, pp. 346–358 (2005), DOI: 10.1109/TPWRD.2004.835039.

[13] Bazelyan E.M., Raizer Y.P., *Lightning Physics and Lightning Protection*, CRC Press, Boca Raton (2000), DOI: 10.1201/9780367801533J.

[14] Shen J., Gong J., Zhou D., *Lightning return stroke positioning method based on CWT narrowband feature extraction*, Atmosphere, vol. 16, no. 302 (2025), DOI: 10.3390/atmos16030302.

[15] Maslowski G., *Corona current concept in lightning return-stroke models of engineering type*, Archives of Electrical Engineering, vol. 59, no. 3–4, pp. 177–188 (2010), DOI: 10.2478/s10171-010-0014-z.

[16] Leśniak P., *Metoda analizy wpływu indywidualnych cech układu „piorun – linia przesyłowa" na wywoływane w niej przepięcia*, PhD Thesis (in Polish), Faculty of Electrical Engineering, Warsaw University of Technology, Warsaw (2017).

[17] Yu J., Gu S., Liu J., Liu H., *Indirect lightning performance of 10-kV overhead distribution lines*, Frontiers Energy Res., vol. 12 (2024), DOI: 10.3389/fenrg.2024.1367183.

[18] Cooray V., Cooray G., Rubinstein M., Rachidi F., *Exact expressions for lightning electromagnetic fields: Application to the Rusck field-to-transmission line coupling model*, Atmosphere, vol. 14, no. 350 (2023), DOI: 10.3390/atmos14020350.

[19] Nucci C.A., Mazzetti C., Rachidi F., Ianoz M., *On lightning return stroke models for LEMP calculations*, 19th International Conference on Lightning Protection, Austrian Electrotech. Assoc., Graz, Austria (1988).

[20] Balanis C.A., *Advanced Engineering Electromagnetics*, New York, NY, USA, Wiley (1989).

[21] Chen H., Liu Q., Li Y., Huang C., Zhang H., Xu Y., *Research on the Method of Near-Field Measurement and Modeling of Powerful Electromagnetic Equipment Radiation Based on Field Distribution Characteristics*, Energies, vol. 16, no. 4 (2023), DOI: 10.3390/en16042005V.

[22] Cooray V., Rachidi F., Rubinstein M., *An Engineering Model to Represent Positive Return Strokes – An Extension of the Modified Transmission Line (MTL) Model*, Atmosphere, vol. 15, 1265 (2024), DOI: 10.3390/atmos15111265.

[23] Munalli D., Dimitrakis G., Chronopoulos D., Greedy S., Long A., *Electromagnetic shielding effectiveness of carbon fibre reinforced composites*, Composites Part B: Engineering, vol. 173, 106906 (2019), DOI: 10.1016/j.compositesb.2019.106906.

[24] Li D. *et al.*, *On Lightning Electromagnetic Field Propagation Along an Irregular Terrain*, in IEEE Transactions on Electromagnetic Compatibility, vol. 58, no. 1, pp. 161–171 (2016), DOI: 10.1109/TEMC.2015.2483018.

[25] Cooray V., Rubinstein M., Rachidi F., *Modified Transmission Line Model with a Current Attenuation Function Derived from the Lightning Radiation Field – MTLD Model*, Atmosphere, vol. 12, 249 (2021), DOI: 10.3390/atmos12020249.

[26] IEEE Std 13092005, *Standard for Calibration of Electromagnetic Field Sensors and Probes, Excluding Antennas, from 9 kHz to 40 GHz*, IEEE Electromagnetic Compatibility Society, New York, NY (2005).

[27] ASTM D493599, *Standard Test Method for Measuring the Electromagnetic Shielding Effectiveness of Planar Materials*, ASTM International, West Conshohocken, PA (1999), withdrawn (2005).

[28] Wilson P.F., Ma M.T., *A Study of Techniques for Measuring the Electromagnetic Shielding Effectiveness of Materials*, NIST Technical Note 1095, National Institute of Standards and Technology, Gaithersburg, MD (1986), DOI: 10.6028/nbs.tn.1095.

[29] Schelkunoff S.A., *Electromagnetic Waves*, D. Van Nostrand Company, Inc., New York, NY (1943).

[30] Paleo A.J., Zille A., Van Hattum F.W., Ares-Pernas A., Moreira J.A., *Maxwell–Garnett modeling of dielectric composites*, Journal of Composite Materials, vol. 53, no. 4, pp. 551–563 (2019), DOI: 10.1177/0021998318806976.

[31] Hong W., Xiao P., Luo H., Li Z., *Microwave axial dielectric properties of carbon fiber*, Scientific Reports, vol. 5, no. 14927 (2015), DOI: 10.1038/srep14927.

[32] Elimat Z.M., Hamideen M.S., Schulte K.I., Wittich H., de la Vega A., Wichmann M., Buschhorn S., *Dielectric properties of epoxy/short carbon fiber composites*, Journal of Materials Science, vol. 45, no. 19, pp. 5196–5203 (2010), DOI: 10.1007/s10853-010-4557-6.

[33] Kim H.C., See S.K., *Electrical properties of unidirectional CFRP composites*, Journal of Materials Science, vol. 35, pp. 2837–2851 (2000), DOI: 10.1023/A:1004815612461.

[34] Chung D.D.L., *Carbon-fiber polymer-matrix composites in the microwave regime*, Journal of Materials Science & Technology, vol. 32, no. 2, pp. 226–232 (2016), DOI: 10.1016/j.jmst.2015.10.010.

[35] Liu X., Yin X., Kong L., Li Q., Liu Y., Duan W., Zhang L., Cheng L., *Fabrication and electromagnetic interference shielding effectiveness of carbon nanotube reinforced carbon fiber/pyrolytic carbon composites*, Carbon, vol. 68, pp. 501–510 (2014), DOI: 10.1016/j.carbon.2013.11.027.

[36] Limbrock J.K., Kemna A., *Relationship between Cole–Cole model parameters in permittivity and conductivity formulation*, Geophysical Journal International, vol. 239, no. 2, pp. 964–970 (2024), DOI: 10.1093/gji/ggae300.

[37] David S., McLachlan D.S., Doyle T.B., Sauti G., *Percolation behaviour in the magnetic permeability and electrical conductivity in conducting magnetic – insulating non magnetic binary composites*, Journal of Magnetism and Magnetic Materials, vol. 458, pp. 365–370 (2018), DOI: 10.1016/j.jmmm.2018.03.002.

[38] Folorunso O., Hamam Y., Sadiku R., Ray S.S., Joseph A.G., *Parametric Analysis of Electrical Conductivity of Polymer-Composites*, Polymers, vol. 11, no. 8, 1250 (2019), DOI: 10.3390/polym11081250.

[39] Munalli D., Dimitrakis G., Chronopoulos D., Greedy S., Long A., *Electromagnetic shielding effectiveness of carbon fibre reinforced composites*, Composites Part B: Engineering, vol. 173, no. 106906 (2019), DOI: 10.1016/j.compositesb.2019.106906.

[40] Munalli D., Dimitrakis G., Chronopoulos D., Greedy S., Long A., *The use of free-space microwave non-destructive techniques: simulation of damage detection in carbon fibre reinforced composites*, Presented at 11th Symposium on NDT in Aerospace, Paris, France (2019).

[41] Tserpes K.I., Tzatzadakis V., Bachmann J., *Electrical Conductivity and Electromagnetic Shielding Effectiveness of Bio-Composites*, Journal of Composites Science, vol. 4. no. 28 (2020), DOI: 10.3390/jcs4010028.